MYC oncogene overexpression drives renal cell carcinoma in a mouse model through glutamine metabolism

Emelyn H. Shroff[a], Livia S. Eberlin[b], Vanessa M. Dang[c], Arvin M. Gouw[a], Meital Gabay[a], Stacey J. Adam[a], David I. Bellovin[a], Phuoc T. Tran[d,e], William M. Philbrick[f], Adolfo Garcia-Ocana[g], Stephanie C. Casey[a], Yulin Li[a], Chi V. Dang[c], Richard N. Zare[b,1], and Dean W. Felsher[a,1]

[a]Division of Medical Oncology, Departments of Medicine and Pathology, and [b]Department of Chemistry, Stanford University School of Medicine, Stanford, CA 94305; [c]Division of Hematology and Oncology, Department of Medicine, Abramson Cancer Center, University of Pennsylvania, Philadelphia, PA 19104; Departments of [d]Radiation Oncology and Molecular Radiation Sciences, and [e]Oncology, The Sidney Kimmel Comprehensive Cancer Center, Johns Hopkins University School of Medicine, Baltimore, MD 21231; [f]Center on Endocrinology and Metabolism, Yale University School of Medicine, New Haven, CT 06520; and [g]Diabetes, Obesity and Metabolism Institute, Icahn School of Medicine at Mount Sinai, New York, NY 10029

Contributed by Richard N. Zare, April 15, 2015 (sent for review March 26, 2015; reviewed by Robert N. Eisenman, Theodore R. Holman, and Evan R. Williams)

The MYC oncogene is frequently mutated and overexpressed in human renal cell carcinoma (RCC). However, there have been no studies on the causative role of MYC or any other oncogene in the initiation or maintenance of kidney tumorigenesis. Here, we show through a conditional transgenic mouse model that the MYC oncogene, but not the RAS oncogene, initiates and maintains RCC. Desorption electrospray ionization–mass-spectrometric imaging was used to obtain chemical maps of metabolites and lipids in the mouse RCC samples. Gene expression analysis revealed that the mouse tumors mimicked human RCC. The data suggested that MYC-induced RCC up-regulated the glutaminolytic pathway instead of the glycolytic pathway. The pharmacologic inhibition of glutamine metabolism with bis-2-(5-phenylacetamido-1,2,4-thiadiazol-2-yl) ethyl sulfide impeded MYC-mediated RCC tumor progression. Our studies demonstrate that MYC overexpression causes RCC and points to the inhibition of glutamine metabolism as a potential therapeutic approach for the treatment of this disease.

MYC oncogene | renal cell carcinoma | desorption electrospray ionization mass spectrometry imaging | glutamine metabolism

Renal cell adenocarcinoma (RCC) is a kidney cancer that originates in the lining of the proximal convoluted tubule, a part of the very small tubes in the kidney that transport waste molecules from the blood to the urine. Most patients who present with advanced RCC have a dismal prognosis because RCC easily metastasizes and advances in therapy have been limited (1–3). A lack of transgenic models of RCC has made it difficult to identify and test new therapeutic modalities.

The *MYC* pathway is activated in most cases of human RCC (4), genomically amplified in 5–10% of patients, overexpressed in 20% (5), and associated with a hereditary RCC syndrome (6) suggesting a causal role in the pathogenesis, but this has never been examined. Here, we report the development of a conditional transgenic mouse model for MYC-deregulated human RCC. The *MYC* oncogene contributes to tumorigenesis of many types of cancer through various mechanisms (7–10), including the regulation of proliferation and growth, protein and ribosomal biogenesis, changes in metabolism, lipid synthesis, and induction of angiogenesis (11–14). MYC reprogramming can result in tumors that are addicted to glucose and/or glutamine for their energy metabolism (15–19). MYC directly regulates specific genes of the glycolytic and glutaminolytic pathways (15, 17, 20, 21), including lactate dehydrogenase A (LDHA), glucose transporter 1 (Glut1), hexokinase 2 (HK2), phosphofructokinase-M 1 (PFKM1), and enolase 1 (Eno1) (21–23). Also, MYC coordinates genes involved in glutamine catabolism (*SI MYC and Glutamine Catabolism*). However, there has been no evidence to show that MYC overexpression directly drives and maintains RCC or how this occurs.

Through our new transgenic mouse model, we showed that transgenic MYC, but not mutant RAS, overexpression in vivo rapidly initiates a highly aggressive RCC that histologically resembles collecting-duct carcinoma, a highly aggressive subtype of RCC. MYC-induced RCC was completely reversible upon MYC suppression in our mouse model. We used high-mass resolution and high-mass accuracy desorption electrospray ionization–mass-spectrometric imaging (DESI-MSI) and molecular biology methods to investigate the changes in metabolites, lipids, proteins, and genes in our RCC model. We used this approach because we previously described the successful use of DESI-MSI and transgenic mouse models to examine the lipid profiles of MYC-induced hepatocellular carcinomas (HCCs) (24) and lymphomas (25).

In DESI-MSI, a tissue sample is bombarded with microdroplets that dissolve hundreds of lipids and metabolites on its surface at a particular location (26). The splash of microdroplets on the tissue surface forms secondary microdroplets that enter a mass spectrometer and provide characterization of the molecules on the tissue surface at that particular location. By moving the sample in two dimensions, we obtain a detailed chemical map of the tissue.

Significance

The absence of appropriate transgenic animal models of renal cell carcinomas (RCCs) has made it difficult to identify and test new therapies for this disease. We developed a new transgenic mouse model of a highly aggressive form of RCC in which tumor growth and regression is conditionally regulated by the MYC oncogene. Using desorption electrospray ionization–mass-spectrometric imaging, we found that certain glycerophosphoglycerols and metabolites of the glutaminolytic pathway were higher in abundance in RCC than in normal kidney tissue. Up-regulation of glutaminolytic genes and proteins was identified by genetic analysis and immunohistochemistry, therefore suggesting that RCC tumors are glutamine addicted. Pharmacological inhibition of glutaminase slowed tumor progression in vivo, which may represent a novel therapeutic route for RCC.

Author contributions: E.H.S., V.M.D., P.T.T., R.N.Z., and D.W.F. designed research; E.H.S., L.S.E., V.M.D., M.G., D.I.B., S.C.C., and Y.L. performed research; L.S.E., W.M.P., A.G.-O., C.V.D., and R.N.Z. contributed new reagents/analytic tools; E.H.S., L.S.E., V.M.D., A.M.G., S.J.A., S.C.C., and R.N.Z. analyzed data; and E.H.S., L.S.E., A.M.G., C.V.D., R.N.Z., and D.W.F. wrote the paper.

Reviewers: R.N.E., Fred Hutchinson Cancer Research Center; T.R.H., University of California, Santa Cruz; and E.R.W., University of California, Berkeley.

The authors declare no conflict of interest.

[1]To whom correspondence may be addressed. Email: zare@stanford.edu or dfelsher@stanford.edu.

This article contains supporting information online at www.pnas.org/lookup/suppl/doi:10.1073/pnas.1507228112/-/DCSupplemental.

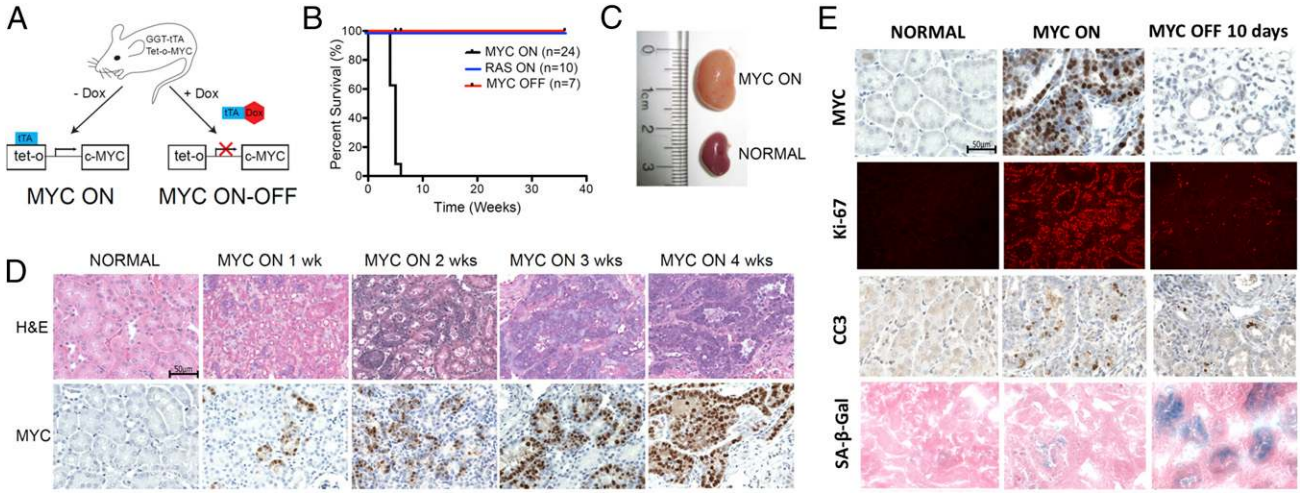

Fig. 1. MYC but not RAS initiates renal tumorigenesis. (*A*) Transgenic mice with the γ-glutamyl transferase (GGT) promoter driving the tetracycline transactivator protein (tTA) and MYC under the control of the tetracycline-responsive element generates MYC-GGT-tTA mice. (*B*) Kaplan–Meier overall survival analysis of mice with MYC ($n = 27$) or K-RAS ($n = 7$) transgene. ON indicates activated oncogenes, and OFF indicates oncogene was never activated. (*C*) Gross anatomy of a MYC-GGT-tTA kidney after 4 wk of MYC activation compared with control where MYC remain inactivated. (*D*) Weekly serial H&E and MYC IHC of kidney sections following MYC activation. (*E*) Representative IHC and immunofluorescence images showing protein expression and histological changes upon MYC activation and inactivation for 10 d. For all quantification, $n = 3$ mice were examined at each time point.

By using DESI-MSI, we found a previously unidentified lipid signature characteristic of MYC-induced RCC. The majority of the molecular ions were identified by tandem and high-resolution mass spectrometry as free fatty acids and complex glycerophospholipids. Interestingly, many of the glycerophospholipids found in higher relative abundance in MYC-induced RCC were ones previously observed in MYC-induced HCC and lymphomas.

Furthermore, to investigate the relationship between MYC and glutamine metabolism, we used DESI-MSI to image the distribution of specific metabolites of the glutaminolytic pathway. To confirm our results, we measured the abundance of different genes in the glutamine pathway to show that MYC-induced RCC expressed glutamine pathway genes. Furthermore, these tumors were highly addicted to glutamine. To evaluate whether these pathways have therapeutic value, we performed pharmacological inhibition of glutaminase, which converts glutamine to glutamate for its further oxidation through the TCA cycle. The inhibition of glutaminase by bis-2-(5-phenylacetamido-1,2,4-thiadiazol-2-yl)ethyl sulfide (BPTES) (27) slowed RCC tumor progression, suggesting that targeting the glutaminolytic pathway is a potential therapeutic approach to treat human RCC (24, 25).

Results

MYC, Not RAS, Initiated RCC. There are no autochthonous mouse models of RCC. Based on prior reports suggesting a role for MYC in the pathogenesis of RCC (4–6), we used the Tet system to regulate the expression of the Tet-O-MYC (7) or Tet-O-K-RAS (kindly provided by H. Varmus, NIH, Bethesda, MD). The expression of the oncogene was driven by the kidney-specific γ-glutamyl transferase gene promoter (GGT) (28) coupled to the tetracycline transactivating gene (tTA) (Fig. 1*A*). Transgenic mice conditionally expressed MYC or RAS in the proximal convoluted tubule cells of the kidney when doxycycline (Dox) was removed from the drinking water; the conditional expression was confirmed by immunohistochemistry (IHC) for MYC or Western blot analysis for mutant K-RAS (Fig. 1*B* and Fig. S1*A*, respectively). Induction of MYC, but not K-RAS, expression increased kidney size (Fig. 1*C*), which was associated histologically with rapidly progressing RCC (Fig. 1*D*). Hence, MYC, but not K-RAS, can initiate renal cell tumorigenesis.

MYC-induced tumors were evaluated for makers of RCC by IHC. Tumors expressed PAX8, a marker for kidney cancers (29, 30) (Fig. S2, panel 1), as well as E-cadherin (Fig. S2, panel 2), which indicated an epithelial origin. The tumors stained positive for CK5/6 and CK7 (Fig. S2, panels 3 and 4) but not for CK20 (Fig. S2, panel 5), indicating that the subtype was of the collecting-duct carcinoma (30). Evaluation by two pathologists concurred that the profile of kidney tumor markers was consistent with RCC originating from the collecting duct, a rare subtype of lethal RCC (31). Despite the rarity of this type of renal cancer, this transgenic mouse provides a unique means to study a highly aggressive form RCC in vivo and is a tool to discover new therapeutic options.

MYC-Induced RCC Was Reversible. The MYC-driven tumors were reversible upon oncogene suppression with Dox treatment (Fig. 1*E*). The reversal was confirmed by looking for changes in proliferation, apoptosis, senescence, and angiogenesis (7–9, 12–14). The MYC inactivation was associated with complete regression of RCC that could be quantitatively demonstrated by serial weekly MRI imaging as well as by histological examination of hematoxylin and eosin (H&E)-stained tissue sections (Fig. 1*E* and Fig. S3 *A* and *B*). MYC protein expression was completely suppressed by 2 d after Dox treatment (Fig. S3*C*, row 1), associated with an eightfold decrease in proliferation as measured by antigen Ki-67 staining (Fig. S3*C*; 54% versus 6.5%, $P < 0.0001$). Notably, apoptosis did not change significantly as measured by cleaved caspase 3 (CC3) (Fig. S3*C*, row 3; 63% at 2 d and 38% at 10 d of MYC inactivation). Cellular senescence exhibited a small decrease at 2 and 5 d, with a much more significant increase 10 d after MYC inactivation (0.7%, 2.3%; $P < 0.0001$), as measured by acidic β-galactosidase staining (SA-β-Gal). However, angiogenesis did not change as measured by CD31 staining (Fig. S4). Thus, it appeared that the RCC tumors regressed because of a marked and rapid inhibition of proliferation accompanied by the persistence of apoptosis (32).

MYC-Induced RCC Exhibited a Distinct Lipid Signature. To investigate the lipid changes in MYC-induced RCC, DESI-MSI analysis was performed in kidney tissue 2 and 4 wk after MYC activation (MYC ON), and then followed by 4 wk of MYC inactivation (MYC OFF). Our analysis was performed in the negative-ion mode in the *m/z* 200–1,000 range, in which a broad variety of free

fatty acids and complex glycerophospholipids of different classes were detected (26). To identify these species, we used tandem mass spectrometry analysis and high-mass accuracy measurements. The fragmentation patterns obtained were compared with what is reported in the literature as characteristic for the different lipid classes (33) and were used in combination with high-mass accuracy measurements for lipid identification. Samples of RCC and normal kidney were imaged using DESI-MSI coupled to a high-mass resolution/mass accuracy mass spectrometer. A solvent mixture of dimethylformamide:acetonitrile (DMF:ACN) (1:1) was used to allow histological evaluation to be performed on the same tissue section and provide unambiguous correlation between molecular signatures and tissue disease state (34).

Select 2D ion images were obtained from a tissue sample of control (normal) kidney, 2-wk MYC-ON induced RCC, 4-wk MYC-ON induced RCC, and 4-wk MYC-OFF induced RCC (Fig. 2). Each tissue section was a full cross-section of the kidney of each animal. After DESI-MSI, the tissue sections were subjected to H&E staining; an optical image of the stained sections is shown in Fig. 2. Note that, by using DMF:ACN as the solvent system, the tissue morphology was preserved in the stained tissue sections after the DESI-MSI process (34). The control kidney exhibited histologically a normal architecture with its two major structures, the outer renal cortex and the inner renal medulla. In the 2-wk MYC-ON kidney, RCC was observed with a high accumulation of neoplastic cells in the central region of the organ. In the 4-wk MYC-ON tissue, the total volume of the kidney was significantly increased, with the destruction of most of the normal architecture of the kidney by neoplastic cells compared with the 2-wk MYC-ON tissue. Many of the ions detected by DESI-MSI were localized within the morphological structures of the kidney. For example, *m/z* 878.601, which was identified as the lipid (3′-sulfo)Galβ-Ceramide(d18:0/22:0(2OH)) was exclusively observed at the renal medulla by DESI-MSI, whereas *m/z* 327.231, identified as docosahexaenoic acid, FA(22:6), was observed with high relative intensity at the renal cortex. Lipids were identified with an absolute mass error of less than 8 ppm. Note that isomerism of the double bonds in the fatty acid (FA) chains of the glycerophospholipids complicates precise structural assignment, which is why FA chains are only tentatively assigned.

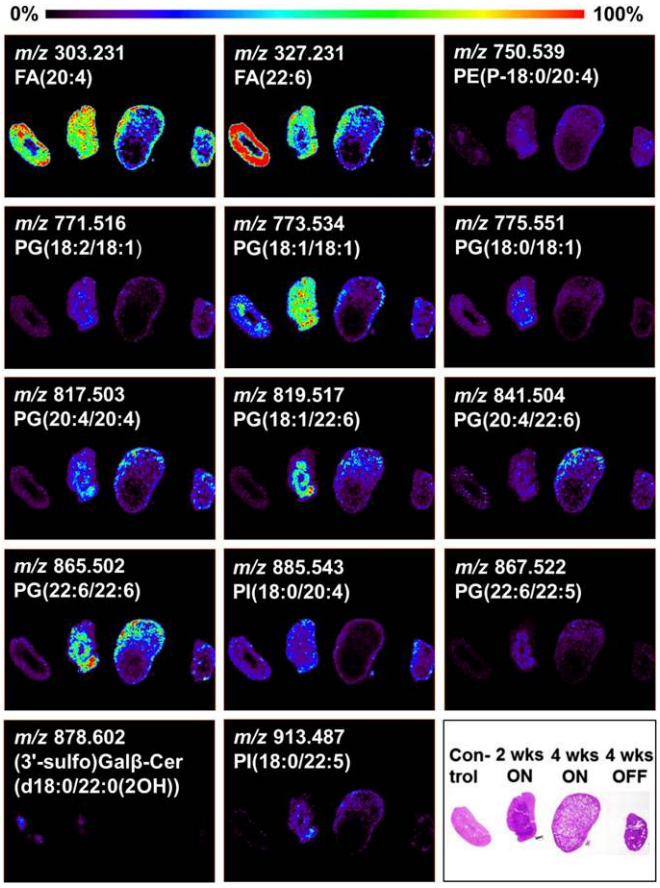

Fig. 2. DESI-MSI of MYC-induced RCC shows specific lipid signature. Representative DESI-MS ion images of cross-sections of control kidney, 2-wk MYC ON kidney, 4-wk MYC ON kidney, and 4-wk MYC OFF kidney, which were analyzed concomitantly, are shown. Images display the 2D distribution of *m/z* 303.2309, *m/z* 327.2308, *m/z* 750.5393, *m/z* 771.5161, *m/z* 773.5344, *m/z* 775.5510, *m/z* 817.5034, *m/z* 819.5196, *m/z* 841.5037, *m/z* 865.5021, *m/z* 885.5432, *m/z* 867.5218, *m/z* 818.6018, and *m/z* 913.4865. The molecular identification of the ions are shown within each panel. The bottom right panel shows an optical image of the tissue sections that were H&E stained after DESI-MSI.

The relative abundances of specific lipids were observed to exhibit striking differences in the spectra of MYC-induced RCC and normal kidney tissues (Fig. S5). High relative abundances of a variety of glycerophosphoglycerols (PGs) were observed in the MYC-ON samples compared with the control kidney samples. In particular, *m/z* 865.502, identified as PG(22:6/22:6), showed a temporal change in its total abundance, with highest relative intensities at 4 wk of MYC activation. DESI-MS ion images of *m/z* 771.516, *m/z* 773.532, *m/z* 775.551, *m/z* 817.503, *m/z* 819.520, *m/z* 865.502, and *m/z* 867.522, which were identified as PG(18:2/18:1), PG(18:1/18:1), PG(18:0/18:1), PG(20:4/20:4), PG(18:1/22:6), PG(22:6/22:6), and PG(22:6/22:5), respectively, are shown in Fig. 2. High intensity of these lipid species was previously observed in both MYC-induced HCC and lymphoma by DESI-MSI (24, 25), which suggests a relationship between MYC oncogene overexpression and PG metabolism. Other lipid species, including *m/z* 303.231, *m/z* 885.543, and *m/z* 747.513, identified as FA(20:4), PI(18:0/20:4), and PG(16:0/18:1), respectively, were observed at similar relative abundances in both RCC and control tissues. Interestingly, the 4-wk MYC-OFF tissue presented a lipid profile similar to the control tissue for the majority of the areas analyzed within the kidney. Nevertheless, DESI-MS ion images revealed small focal areas with high relative abundance of PGs in the 4-wk MYC-OFF induced RCC compared with the control kidney tissue. These focal areas could be related to remaining neoplastic cells.

MYC-Induced RCC Activated Glutamine Metabolism. To further understand how MYC maintained tumorigenesis in RCC, gene expression analysis was performed at 1, 2, and 4 wk after MYC activation. Quantile normalization and $\log_2$ transformation was performed across all samples using >twofold change in gene expression with a cutoff value of $P = 0.05$. Kyoto Encyclopedia of Genes and Genomes (KEGG) is a collection of databases dealing with genomes, biological pathways, diseases, drugs, and chemical substances. KEGG pathway analysis demonstrated changes in the metabolic pathways including up-regulation of alanine, aspartate, and glutamate metabolism, and more complex effects on glycolysis, glycogenesis, and O-glycan biosynthesis. The time-dependent up-regulation of genes encoding nutrient transporters and enzymes of the glutaminolysis pathway was observed (Fig. S6*A*). Although glycolysis was generally decreased, certain glycolytic genes were increased (Fig. S6*B*). MYC regulates glutaminase expression through direct promoter activation or posttranscriptionally through miR-23a/b (17), which was decreased upon MYC activation (Fig. S7 *A* and *B*). IHC analysis confirmed the up-regulation of protein expression of the glutaminolytic pathway (Fig. 3*A*, panels 1 and 2) as well as the down-regulation of the glycolytic pathway (Fig. 3*A*, panels 3 and 4).

Then, DESI-MSI was used to examine the changes in relative abundances of specific metabolites in RCC and control kidney in

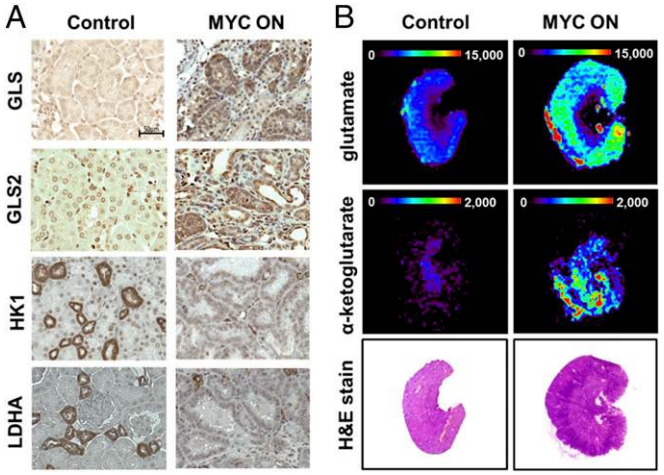

Fig. 3. Glutaminolysis pathway is up-regulated in MYC-induced renal adenocarcinoma. (*A*) IHC showing glutaminase 1 and 2, hexokinase 1, and LDHA expression in normal kidneys (control) and kidneys that have MYC activated for 3 wk. (*B*) Representative DESI-MS ion images of glutamate and α-ketoglutarate at 2-wk MYC activation compared with control. H&E was performed on the same section following DESI-MSI.

situ (32, 35). Metabolites of the glutaminolytic pathway, including glutamate and α-ketoglutarate, were identified, as well as an increase in relative abundances of ions corresponding to citrate, pyruvate, malate, and succinate in RCC compared with control samples. This finding suggests the activation of the Krebs cycle (Fig. S6*C*). DESI-MSI provided a spatial resolution of 200 μm and allowed colocalization of the metabolites with tumor areas within the tissue sections to this precision (Fig. 3*B*). In combination with gene expression results, these results indicate that MYC initiation of RCC was associated with the activation of glutaminolysis.

Inhibition of Glutaminase by BPTES Slowed RCC Tumor Progression. We evaluated the dependency of MYC-induced RCC on glutamine and glucose. First, we derived a cell line (E28) from our transgenic mouse model that continued to conditionally express MYC, as shown by Western blot analysis (Fig. S8*A*). E28 could only proliferate and survive in media supplemented with glutamine (Fig. S9*A*) but not glucose (Fig. S9*B*). Second, we found that genes required for glutamine transport (Fig. S9*C*) and the glutaminolytic pathway markedly decreased after MYC inactivation (Fig. S9*D*).

Next, we evaluated the activity of an allosteric inhibitor of kidney type glutaminase, BPTES (Fig. S10*A*) (27). First, BPTES was found to have in vitro effects on the growth of MYC-induced RCC (Fig. S9*E*). Second, BPTES was examined for antitumor activity in vivo in our transgenic mouse model. BPTES treatment was initiated at 2 wk after MYC activation. Mice were visualized by magnetic resonance imaging at 7 and 14 d following treatment (Fig. S10*B*). BPTES-treated tumors grew less in comparison with control tumors, which were treated with DMSO (11% versus 34%; $P = 0.003$) at 7 d and (49% versus 70%; $P = 0.003$) at 14 d of treatment (Fig. 4 *A* and *B*). Similarly, after 14 d of BPTES treatment, the kidneys weighed 32% ($P = 0.0003$) less than the DMSO-treated kidneys (Fig. 4*C*). The small molecule 3-dihydroxy-6-methyl-7-(phenylmethyl)-4-propylnaphthalene-1-carboxylic acid (FX-11) is known to inhibit LDHA, which is a key part of the glycolytic pathway (36). In separate experiments, we found that FX-11 had no apparent influence on tumor growth or kidney weight even when given at doses that can affect P493 xenografts, which are models for a lymphoma conditionally driven by MYC (37).

Histological examination revealed that the BPTES treatment was associated with a reduction in the neoplastic cells, whereas DMSO and FX-11 had no effect on reducing neoplastic cells (Fig. S10*C*). Furthermore, we observed a 50% decrease in kidney cell proliferation of BPTES-treated mice compared with DMSO-treated mice by Ki-67 immunofluorescence staining (Fig. S11 *A*, row 1, and *B*). There was no change in apoptosis as measured by CC3 staining upon MYC inactivation (Fig. S11*A*, row 2) or in BPTES-treated mice (Fig. S11*C*). These results indicate that inhibition of glutaminolysis impedes MYC-induced RCC. Hence, in this transgenic model, MYC appears to be generally programming glutamine metabolism and relying less on glucose metabolism (38, 39).

MYC and Glutaminase Are Overexpressed in Human RCC. Finally, we asked whether MYC and glutaminase protein expression are associated in human tumors from Stanford Tissue Bank and the Stanford's Department of Pathology. By IHC, MYC is expressed in all samples; however, the collecting-duct carcinomas had a significantly higher expression level (Fig. 5). We observed that glutaminase is expressed in all collecting-duct carcinoma samples but only expressed in 60% of clear-cell carcinoma (ccRCC GLS+) tumor tissue tested. Our data are therefore suggestive that a subset of human clear-cell carcinoma may use glutaminolysis as the preferential pathway for energy supply.

Discussion

We generated a conditional transgenic mouse model of human MYC-driven RCC (5, 6), thus providing an in vivo demonstration that MYC can induce and its sustained expression is required to maintain RCC. Our results are consistent with prior observations that the MYC pathway is active, the gene is often amplified and overexpressed, and genomic alteration is associated with a hereditary RCC (4–6). These MYC-induced tumors exhibit the phenotypic features of a highly aggressive subtype of tumors, renal cell collecting-duct carcinoma (40). MYC inactivation reversed their neoplastic features associated with arrest, apoptosis, and senescence. RCC has been associated with mutations in many gene products, such as tumor suppressor genes, the Von Hippel–Lindau (VHL) gene and oncogenes such as the tyrosine kinase receptor (MET) (3, 41–48) and mutation of PI3K (5). Notably, PI3K appears to maintain neoplasia via MYC (49). MYC also has been shown to be genetically activated

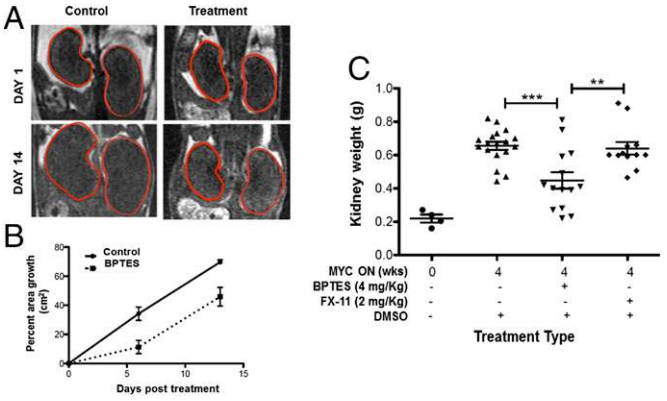

Fig. 4. Inhibition of glutaminase impedes MYC-induced renal tumorigenesis in vivo. (*A*) Representation of weekly MRI scans of a BPTES-treated mouse and a DMSO-treated mouse over 2 wk. (*B*) Percent area growth derived from MRI of tumors undergoing BPTES ($n = 8$) or DMSO ($n = 8$) treatment. (*C*) Final weight of kidneys treated with BPTES ($n = 14$), FX-11 ($n = 12$), or DMSO ($n = 18$) after 4 wk of MYC activation compared with MYC inactivation.

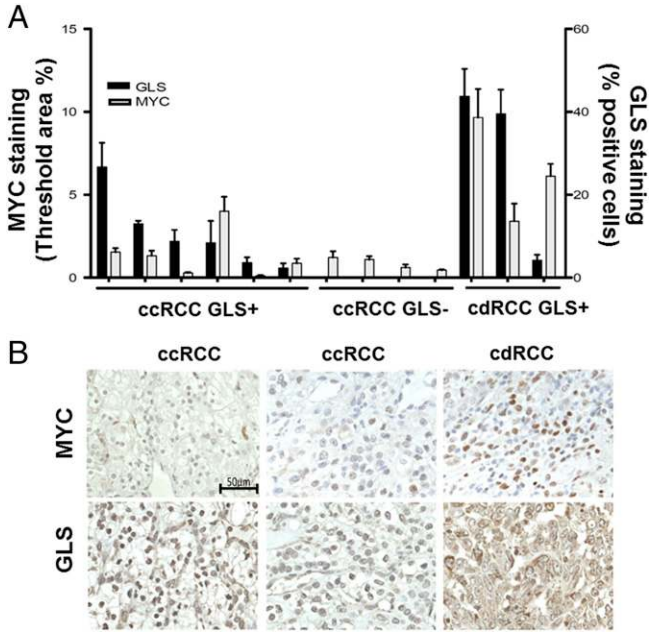

Fig. 5. MYC and glutaminase are overexpressed in human RCC. (*A*) Quantification of IHC staining of glutaminase (GLS) (black bars) and MYC (gray bars) in clear-cell RCC (ccRCC) and collecting-duct RCC (cdRCC) human samples. (*B*) Representative GLS and MYC staining in ccRCC and cdRCC human samples.

in subset of RCC, and its overexpression is more common in RCC, but its causal role has not been examined experimentally (40, 50–54). We establish here that MYC can cause RCC in a conditional transgenic mouse model and its inactivation can induce sustained tumor regression. In contrast, activated K-RAS, another oncogene, is neither found in human RCC nor is it sufficient to induce RCC in the mouse, illustrating the tissue-specific effects of activated oncogenes.

We generated an autochthonous transgenic mouse model of RCC, which should be generally useful for developing new therapeutics. Using DESI-MSI, we identified complex lipids that were present in higher relative abundance in MYC-ON RCC tissue compared with control kidney and MYC-OFF tissues. The majority of the lipid species was identified as PGs. Interestingly, the changes in lipid profiles detected by DESI-MSI were previously reported in human RCC. In particular, higher relative abundance of PG(18:1/18:1) was observed in human RCC compared with adjacent normal kidney tissue (55). PGs are present at low levels (1–2%) in most nonneoplastic animal tissue and can serve as the precursor of cardiolipins, which are complex lipids found almost exclusively in mitochondrial membranes (56). This increase in PGs observed in RCC and other MYC-induced carcinomas is consistent with MYC's induction of mitochondrial biogenesis (57), as related to the Warburg cancer theory (58). Importantly, MYC may increase lipids through MondoA (MLXIP) to increase SREBP-1, thereby inducing key lipogenic genes: FASN and SCD (59). This in turn would increase fatty acids (60), required for the synthesis of more complex phospholipids. We previously observed high abundances of PGs in MYC-induced HCC and lymphomas. Hence, our results here further indicate a relationship between MYC expression and PG metabolism.

Furthermore, we used DESI-MSI to assess the changes in the abundances of specific glutaminolytic metabolites in situ. Gene expression analysis of our transgenic mouse model suggested that the glutamine pathway was up-regulated but not the glucose pathway. These results indicate that renal carcinoma cells were addicted to glutamine as an energy source.

The inhibition of glutaminase by BPTES halted the growth of MYC-induced RCC both in vitro and in vivo and caused proliferative arrest. BPTES is a selective inhibitor of glutaminase 1 (27, 61, 62). Our results suggest that inhibition of glutaminase 1 can have an antitumorigenic effect on RCC and that MYC-associated RCC is glutamine addicted. However, glutaminase 2, which is not responsive to BPTES, was also activated by MYC in this model; the lack of a more robust inhibition of tumorigenesis in vivo could have resulted from glutaminase 2 providing an escape mechanism. We found that inhibition of glucose metabolism had almost no effect on tumor growth. We suggest that inhibition of glutamine metabolism may be a previously unidentified therapeutic approach for the treatment of RCC associated with MYC overexpression.

Materials and Methods

All animal experiments were performed under the guidelines established by the Administrative Panel on Laboratory Animal Care at Stanford University. Primary renal tumors of GGT-tTa × tet-O-MYC/p53$^{+/-}$ double-transgenic mice were serially passaged three times s.c. through SCID mice. Flow cytometry data were analyzed using FlowJo software (Tree Star). RNA analysis via quantitative real-time PCR was quantified by fluorescence using the ABI Prism 7900HT Sequence Detection System (Applied Biosystems). H&E and immunohistochemical staining was performed using standard procedures. Pictures were then quantified using MetaMorph. Mice were sequentially imaged using a 7 Tesla MRI system at Stanford Small Animal Imaging Center. mRNA expression profiling was performed by the Stanford Functional Genomics Facility using Illumina Mouse WG6 mouse bead arrays. A lab-built DESI-MSI source coupled to an LTQ-Orbitrap XL mass spectrometer (Thermo Scientific) was used for tissue imaging. DESI-MSI was performed in the negative ion mode from *m/z* 90–1200, using the Orbitrap as the mass analyzer at a resolving power of 60,000. The spatial resolution of the imaging experiments was of 200 μm. Additional details regarding the methods of analysis of transgenic mice, imaging, and DESI-MSI analysis are provided in *SI Materials and Methods*.

ACKNOWLEDGMENTS. We thank members of the laboratories of D.W.F. and R.N.Z. for their helpful suggestions toward this manuscript, John Higgings for generously providing us with paraffin section of human collecting-duct carcinoma, Jesse McKenney and Marston Linehan for evaluating this kidney tumor as collecting-duct carcinoma, and Sylvia Plevritis and Ramesh Nair for providing us assistance with the microarray data analysis. We are grateful to members of the Stanford Small Animal Imaging Center for their assistance with MRI, Pauline Chu for generating histology samples, and Norm Cyr for his assistance with microscopy. This work was funded by Burroughs Welcome Fund Career Award; the Damon Runyon Foundation Lilly Clinical Investigator Award; NIH R01 Grants CA 089305, 105102, and 170378; National Cancer Institute (NCI) In Vivo Cellular and Molecular Imaging Center Grant CA 114747; Integrative Cancer Biology Program Grants CA 112973 and U01 CA188383; NIH/NCI P01 Grant CA034233; The Leukemia and Lymphoma Society Translational Research Grant R6223-07 (to D.W.F.); NIH Grant CA 184384 (to R.N.Z. and D.W.F.); American Lung Association Grant RT-169741-N (to E.H.S.); and L'Oréal for Women in Science (L.S.E.).

1. Jemal A, Siegel R, Xu J, Ward E (2010) Cancer statistics, 2010. *CA Cancer J Clin* 60(5):277–300.
2. Zini L, et al. (2009) Population-based assessment of survival after cytoreductive nephrectomy versus no surgery in patients with metastatic renal cell carcinoma. *Urology* 73(2):342–346.
3. Linehan WM, et al. (2004) Genetic basis of cancer of the kidney: Disease-specific approaches to therapy. *Clin Cancer Res* 10(18 Pt 2):6282S–6289S.
4. Tang SW, et al. (2009) MYC pathway is activated in clear cell renal cell carcinoma and essential for proliferation of clear cell renal cell carcinoma cells. *Cancer Lett* 273(1):35–43.
5. Anonymous; Cancer Genome Atlas Research Network (2013) Comprehensive molecular characterization of clear cell renal cell carcinoma. *Nature* 499(7456):43–49.
6. Drabkin HA, et al. (1985) Translocation of c-*myc* in the hereditary renal cell carcinoma associated with a t(3;8)(p14.2;q24.13) chromosomal translocation. *Proc Natl Acad Sci USA* 82(20):6980–6984.
7. Felsher DW, Bishop JM (1999) Reversible tumorigenesis by MYC in hematopoietic lineages. *Mol Cell* 4(2):199–207.
8. Felsher DW, Bishop JM (1999) Transient excess of MYC activity can elicit genomic instability and tumorigenesis. *Proc Natl Acad Sci USA* 96(7):3940–3944.
9. Arvanitis C, Felsher DW (2005) Conditionally MYC: Insights from novel transgenic models. *Cancer Lett* 226(2):95–99.
10. Jain M, et al. (2002) Sustained loss of a neoplastic phenotype by brief inactivation of MYC. *Science* 297(5578):102–104.

11. Dang CV (1999) c-Myc target genes involved in cell growth, apoptosis, and metabolism. *Mol Cell Biol* 19(1):1–11.
12. Rakhra K, et al. (2010) $CD4^+$ T cells contribute to the remodeling of the microenvironment required for sustained tumor regression upon oncogene inactivation. *Cancer Cell* 18(5):485–498.
13. Giuriato S, et al. (2006) Sustained regression of tumors upon MYC inactivation requires p53 or thrombospondin-1 to reverse the angiogenic switch. *Proc Natl Acad Sci USA* 103(44):16266–16271.
14. van Riggelen J, et al. (2010) The interaction between Myc and Miz1 is required to antagonize TGFbeta-dependent autocrine signaling during lymphoma formation and maintenance. *Genes Dev* 24(12):1281–1294.
15. Wise DR, et al. (2008) Myc regulates a transcriptional program that stimulates mitochondrial glutaminolysis and leads to glutamine addiction. *Proc Natl Acad Sci USA* 105(48):18782–18787.
16. Dang CV, Le A, Gao P (2009) MYC-induced cancer cell energy metabolism and therapeutic opportunities. *Clin Cancer Res* 15(21):6479–6483.
17. Gao P, et al. (2009) c-Myc suppression of miR-23a/b enhances mitochondrial glutaminase expression and glutamine metabolism. *Nature* 458(7239):762–765.
18. Le A, et al. (2010) Inhibition of lactate dehydrogenase A induces oxidative stress and inhibits tumor progression. *Proc Natl Acad Sci USA* 107(5):2037–2042.
19. Le A, et al. (2012) Glucose-independent glutamine metabolism via TCA cycling for proliferation and survival in B cells. *Cell Metab* 15(1):110–121.
20. Dang CV (2013) MYC, metabolism, cell growth, and tumorigenesis. *Cold Spring Harb Perspect Med* 3(8):pii: a014217.
21. Kim JW, et al. (2004) Evaluation of myc E-box phylogenetic footprints in glycolytic genes by chromatin immunoprecipitation assays. *Mol Cell Biol* 24(13):5923–5936.
22. Shim H, et al. (1997) c-Myc transactivation of LDH-A: Implications for tumor metabolism and growth. *Proc Natl Acad Sci USA* 94(13):6658–6663.
23. Osthus RC, et al. (2000) Deregulation of glucose transporter 1 and glycolytic gene expression by c-Myc. *J Biol Chem* 275(29):21797–21800.
24. Perry RH, et al. (2013) Characterization of MYC-induced tumorigenesis by in situ lipid profiling. *Anal Chem* 85(9):4259–4262.
25. Eberlin LS, et al. (2014) Alteration of the lipid profile in lymphomas induced by MYC overexpression. *Proc Natl Acad Sci USA* 111(29):10450–10455.
26. Eberlin LS, Ferreira CR, Dill AL, Ifa DR, Cooks RG (2011) Desorption electrospray ionization mass spectrometry for lipid characterization and biological tissue imaging. *Biochim Biophys Acta* 1811(11):946–960.
27. Robinson MM, et al. (2007) Novel mechanism of inhibition of rat kidney-type glutaminase by bis-2-(5-phenylacetamido-1,2,4-thiadiazol-2-yl)ethyl sulfide (BPTES). *Biochem J* 406(3):407–414.
28. Fiaschi-Taesch NM, et al. (2004) Prevention of acute ischemic renal failure by targeted delivery of growth factors to the proximal tubule in transgenic mice: The efficacy of parathyroid hormone-related protein and hepatocyte growth factor. *J Am Soc Nephrol* 15(1):112–125.
29. Ozcan A, et al. (2011) PAX 8 expression in non-neoplastic tissues, primary tumors, and metastatic tumors: A comprehensive immunohistochemical study. *Mod Pathol* 24(6): 751–764.
30. Truong LD, Shen SS (2011) Immunohistochemical diagnosis of renal neoplasms. *Arch Pathol Lab Med* 135(1):92–109.
31. Chao D, et al. (2002) Collecting duct renal cell carcinoma: Clinical study of a rare tumor. *J Urol* 167(1):71–74.
32. Tran PT, et al. (2011) Survival and death signals can predict tumor response to therapy after oncogene inactivation. *Sci Transl Med* 3(103):103ra199.
33. Chan S, Reinhold VN (1994) Detailed structural characterization of lipid A: Electrospray ionization coupled with tandem mass spectrometry. *Anal Biochem* 218(1): 63–73.
34. Eberlin LS, et al. (2011) Nondestructive, histologically compatible tissue imaging by desorption electrospray ionization mass spectrometry. *ChemBioChem* 12(14):2129–2132.
35. Morris ZS, McClatchey AI (2009) Aberrant epithelial morphology and persistent epidermal growth factor receptor signaling in a mouse model of renal carcinoma. *Proc Natl Acad Sci USA* 106(24):9767–9772.
36. Yu Y, et al. (2001) Selective active site inhibitors of human lactate dehydrogenases A4, B4, and C4. *Biochem Pharmacol* 62(1):81–89.
37. Dutta P, et al. (2013) Evaluation of LDH-A and glutaminase inhibition in vivo by hyperpolarized 13C-pyruvate magnetic resonance spectroscopy of tumors. *Cancer Res* 73(14):4190–4195.
38. Chan DA, et al. (2011) Targeting GLUT1 and the Warburg effect in renal cell carcinoma by chemical synthetic lethality. *Sci Transl Med* 3(94):94ra70.
39. Li B, et al. (2014) Fructose-1,6-bisphosphatase opposes renal carcinoma progression. *Nature* 513(7517):251–255.
40. Liu G, Cheresh P, Kamp DW (2013) Molecular basis of asbestos-induced lung disease. *Annu Rev Pathol* 8:161–187.
41. Seizinger BR, et al. (1988) Von Hippel-Lindau disease maps to the region of chromosome 3 associated with renal cell carcinoma. *Nature* 332(6161):268–269.
42. Gnarra JR, et al. (1994) Mutations of the VHL tumour suppressor gene in renal carcinoma. *Nat Genet* 7(1):85–90.
43. Schmidt LS, et al. (2001) Birt-Hogg-Dubé syndrome, a genodermatosis associated with spontaneous pneumothorax and kidney neoplasia, maps to chromosome 17p11.2. *Am J Hum Genet* 69(4):876–882.
44. Tomlinson IP, et al.; Multiple Leiomyoma Consortium (2002) Germline mutations in FH predispose to dominantly inherited uterine fibroids, skin leiomyomata and papillary renal cell cancer. *Nat Genet* 30(4):406–410.
45. Chen J, et al. (2008) Deficiency of FLCN in mouse kidney led to development of polycystic kidneys and renal neoplasia. *PLoS One* 3(10):e3581.
46. Vanharanta S, et al. (2004) Early-onset renal cell carcinoma as a novel extraparaganglial component of SDHB-associated heritable paraganglioma. *Am J Hum Genet* 74(1):153–159.
47. Baysal BE, et al. (2000) Mutations in SDHD, a mitochondrial complex II gene, in hereditary paraganglioma. *Science* 287(5454):848–851.
48. Bjornsson J, Short MP, Kwiatkowski DJ, Henske EP (1996) Tuberous sclerosis-associated renal cell carcinoma. Clinical, pathological, and genetic features. *Am J Pathol* 149(4): 1201–1208.
49. Liu P, et al. (2011) Oncogenic PIK3CA-driven mammary tumors frequently recur via PI3K pathway-dependent and PI3K pathway-independent mechanisms. *Nat Med* 17(9):1116–1120.
50. Beroukhim R, et al. (2009) Patterns of gene expression and copy-number alterations in Von Hippel–Lindau disease-associated and sporadic clear cell carcinoma of the kidney. *Cancer Res* 69(11):4674–4681.
51. Tang SW, Lin JY (2012) Full-length enrich c-DNA libraries-clear cell-renal cell carcinoma. *J Oncol* 2012:680796.
52. Furge KA, et al. (2007) Detection of DNA copy number changes and oncogenic signaling abnormalities from gene expression data reveals MYC activation in high-grade papillary renal cell carcinoma. *Cancer Res* 67(7):3171–3176.
53. Yamamura S, et al. (2012) MicroRNA-34a suppresses malignant transformation by targeting c-Myc transcriptional complexes in human renal cell carcinoma. *Carcinogenesis* 33(2):294–300.
54. Gordan JD, et al. (2008) HIF-alpha effects on c-Myc distinguish two subtypes of sporadic VHL-deficient clear cell renal carcinoma. *Cancer Cell* 14(6):435–446.
55. Dill AL, et al. (2010) Multivariate statistical differentiation of renal cell carcinomas based on lipidomic analysis by ambient ionization imaging mass spectrometry. *Anal Bioanal Chem* 398(7-8):2969–2978.
56. Wallace DC (2012) Mitochondria and cancer. *Nat Rev Cancer* 12(10):685–698.
57. Li F, et al. (2005) Myc stimulates nuclearly encoded mitochondrial genes and mitochondrial biogenesis. *Mol Cell Biol* 25(14):6225–6234.
58. Kiebish MA, Han X, Cheng H, Chuang JH, Seyfried TN (2008) Cardiolipin and electron transport chain abnormalities in mouse brain tumor mitochondria: Lipidomic evidence supporting the Warburg theory of cancer. *J Lipid Res* 49(12):2545–2556.
59. Carroll PA, et al. (2015) Deregulated Myc requires MondoA/Mlx for metabolic reprogramming and tumorigenesis. *Cancer Cell* 27(2):271–285.
60. Morrish F, et al. (2010) Myc-dependent mitochondrial generation of acetyl-CoA contributes to fatty acid biosynthesis and histone acetylation during cell cycle entry. *J Biol Chem* 285(47):36267–36274.
61. Shukla K, et al. (2012) Design, synthesis, and pharmacological evaluation of bis-2-(5-phenylacetamido-1,2,4-thiadiazol-2-yl)ethyl sulfide 3 (BPTES) analogs as glutaminase inhibitors. *J Med Chem* 55(23):10551–10563.
62. DeLaBarre B, et al. (2011) Full-length human glutaminase in complex with an allosteric inhibitor. *Biochemistry* 50(50):10764–10770.